Nucleus accumbens-linked executive control networks mediating reversal learning in tree shrew brain

Ting-Ting Pan[1,2,3,#], Chao Liu[3,6,#], De-Min Li[1,#], Bin-Bin Nie[2], Tian-Hao Zhang[2], Wei Zhang[2,5], Shi-Lun Zhao[2,5], Qi-Xin Zhou[3,6], Hua Liu[2,*], Gao-Hong Zhu[4,*], Lin Xu[3,6,7,*], Bao-Ci Shan[2,5,*]

[1]School of Physics and Microelectronics, Zhengzhou University, Zhengzhou, Henan 450001, China

[2]Beijing Engineering Research Center of Radiographic Techniques and Equipment, Institute of High Energy Physics, Chinese Academy of Sciences, Beijing 100049, China

[3]CAS Key Laboratory of Animal Models and Human Disease Mechanisms, and KIZ-SU Joint Laboratory of Animal Model and Drug Development, and Laboratory of Learning and Memory, Kunming Institute of Zoology, Chinese Academy of Sciences, Kunming, Yunnan 650223, China

[4]Department of Nuclear Medicine, First Affiliated Hospital of Kunming Medical University, Kunming, Yunnan 650032, China

[5]School of Nuclear Science and Technology, University of Chinese Academy of Sciences, Beijing 100049, China

[6]Kunming College of Life Science, University of Chinese Academy of Sciences, Kunming, Yunnan 650204, China

[7]CAS Centre for Excellence in Brain Science and Intelligent Technology, Shanghai 200031, China

[#]Authors contributed equally to this work

[*]Corresponding authors, E-mail: liuhua@ihep.ac.cn; 1026909611@qq.com; lxu@vip.163.com; shanbc@ihep.ac.cn

Supplementary Materials

Animals

Domesticated adult male tree shrews (n=19, aged 8–12 months) were obtained from the breeding colony at the Animal House Center of the Kunming Institute of Zoology (Yunnan, China). The tree shrews were housed individually in a temperature-regulated room (25–27 ℃) with a regular day/night cycle (08:00–20:00). All animals had free access to water and food. The use and care of animals in this study conformed to the international guidelines and protocols approved by the Animal Care and Use Committee of the Kunming Institute of Zoology, Chinese Academy of Sciences (SMKX-20180806-177).

^{18}F-FDG Micro-PET/CT scanning and analysis

Four micro-PET/CT scans were performed during the baseline, learning expert (LE), reversal naive (RN), and reversal expert (RE) stages, respectively (Figure 1A). After intraperitoneal injection of 18F-FDG (185 MBq/kg), the animals were allowed to freely move around the experimental chamber without task as the baseline, or were subjected to a visual discrimination task (LE, RN, and RE) for 30 min. The tree shrews were then anesthetized with isoflurane (5% for induction and 1.5%–2.0% for maintenance) plus medical oxygen and placed in a prone position on the scanning bed of an E-plus 166 micro-PET/CT scanner (Institute of High Energy Physics, CAS, Beijing, China) (Huang et al, 2018). Scanning was performed for 20 min. The PET images were then reconstructed using the two-dimensional ordered subset expectation maximization algorithm with corrections for decay, normalization, dead time, photon attenuation, scatter, and random coincidence. The reconstructed image matrix size was 256×256×63 with a voxel size of 0.5×0.5×1.0 mm^3.

All images were preprocessed using an improved toolbox for voxel-wise analysis of tree shrew brain images based on SPM8 (Welcome Department of Cognitive Neurology) (Huang et al, 2018). Image preprocessing was performed as follows: (1) individual images of tree shrews were spatially normalized into stereotaxic space, (2) normalized images were smoothed with a 2.0×4.5×2.0 mm^3 Gaussian kernel, and (3) image intensity was globally normalized for each image.

Seed-based whole-brain metabolic connectivity analysis

A two-sample *t*-test was used to detect brain regions with significant differences in metabolism at the voxel level between different cognitive stages. The seed region of the reversal learning (RL) network was selected from clusters with significant metabolic differences between the RN and LE stages. To obtain specific spatial metabolic connectivity patterns of the seed regions, voxel-wise Pearson correlation coefficients were calculated between the seed region and all brain voxels based on brain metabolic imaging of the RN stage in an inter-subject manner (Carbonell et al, 2014; Tsai et al, 2020). After false discovery rate (FDR) correction, clusters in the generated brain-wide connectivity map were considered as brain regions highly correlated with the seed region. These brain regions constituted a potential metabolic network associated with visual discrimination RL.

Network analysis

The specificity of a functional network is often demonstrated by longitudinal comparisons of properties of networks across different cognitive states (Huang et al, 2020).

Average network degree (*K*)

The average degree of a network is commonly used as a measure of density, known as the network's total 'wiring cost', to assess the correlation strength of network internode connections (Huang et al, 2020). Average network degree was calculated as follows:

$$K = \frac{1}{N}\sum_i k_i$$

where K_i is the sum of weights attached to node *i* and *N* is the number of nodes.

Global efficiency (E_{glob})

Global efficiency measures the global information transfer ability of a network (Rubinov & Sporns, 2010) and is commonly used as a measure of network integration. Global network efficiency can be measured as:

$$E_{glob} = \frac{1}{N(N-1)}\sum_{i\neq j}\frac{1}{d_{ij}}$$

where d_{ij} is the shortest weighted path length between nodes *i* and *j*.

Synchronization (*S*)

Synchronization refers to the property of a network to synchronize in dynamics among coupled oscillators, which measures how likely it is that all nodes fluctuate in the same wave pattern. This property can be measured as (Wang et al, 2011):

$$S = \frac{\lambda_2}{\lambda_N}$$

where λ_2 and λ_N are the second smallest and largest eigenvalues of the coupling matrix *G*, respectively, defined as (Barahona & Pecora, 2002; Motter et al, 2005):

$$G_{ij}^W = \delta_{ij}\sum_{j=1}^{N} w_{ij} - w_{ij}$$

where w_{ij} is the $(i, j)^{\text{th}}$ element in the weighted network of *W*.

RL network responding to "rule-switch"

To examine the specificity of the potential RL metabolic network in tree shrews, we constructed the networks at the baseline, LE, RN, and RE stages (Supplementary Figure S5A-D). The average network degree (*K*) was significantly higher in RN than in the other stages (***P<0.001, permutation test; Supplementary Figure S5E). Global efficiency of the RL network was significantly higher in RN than in the other stages (***P<0.001, permutation test; Supplementary Figure S5F). In addition, synchronization of the RL network was higher in RN than in the other stages, and significantly higher than that in the LE stage (**P<0.01, permutation test; Supplementary Figure S5G).

Composition of potential metabolic network associated with visual discrimination learning

The seed region of the learning network was selected from clusters with significant metabolic differences between the LE and baseline stages. Compared with the baseline stage, the LE tree shrews completed the visual discrimination learning task, with the probability that they touched the correct picture remaining above 85%. Based on two-sample *t*-test, a cluster located in the left entorhinal cortex (Ent) showed significantly elevated FDG uptake ($P<0.05$, family-wise error (FWE)-corrected; Supplementary Figure S2B, Supplementary Table S3). Furthermore, the standard uptake value ratio (SUVR) of this cluster showed a significant positive correlation with the measured behavior (correct rate) of the tree shrews ($r=0.405$; $P=0.004$, Pearson correlation analysis; Supplementary Figure S3B). Therefore, this cluster was selected as the seed region to explore the network involved in the visual discrimination learning task. A brain-wide metabolic connectivity map of the seed region was generated across subjects based on FDG-PET brain images in the LE stage. Brain clusters with suprathreshold metabolic connection strength were considered to constitute the potential learning network ($P<0.05$, FDR-corrected; Supplementary Figure S6A-B). The masks of the network members were given specific indices to generate a digital atlas of functional metabolic networks associated with visual discrimination learning (Supplementary Figure S6C). Details on the functional network members of visual discrimination learning are presented in Supplementary Table S4.

According to the differences between the RE and baseline stages (Supplementary Figure S2C, Supplementary Table S5), we selected the left Ent as the seed region to explore brain-wide metabolic connectivity based on PET images acquired in the RE stage (Supplementary Figure S7). Details on members of the visual discrimination learning metabolic network in the RE stage are shown in Supplementary Table S6.

Potential metabolic network associated with visual discrimination learning responding to task stages

To examine the specific responses of the potential visual discrimination learning network to task stages, we examined the properties of the learning network in the baseline, LE, RN, and RE stages. As shown in the network connection strength schematic, metabolic correlations among nodes of the learning network in the LE, RN, and RE stages were stronger than those in baseline (Supplementary Figure S8A-D). Permutation tests revealed that the average network degree (K) was significantly higher in the LE, RN, and RE stages than in baseline (***$P<0.001$, permutation test; Supplementary Figure S8E). Global efficiency of the learning network in the LE, RN, and RE stages was significantly higher than in baseline (**$P<0.01$, ***$P<0.001$, permutation test; Supplementary Figure S8F). Additionally, synchronization of the learning network was also higher in the task stages than in the resting stage, with synchronization in the LE and RE stages significantly higher than that in the baseline stage (*$P<0.05$, permutation test; Supplementary Figure S8G). In brief, relative to the resting stage, the learning network exhibited significantly high connectivity and functional consistency in the task stages, indicating the specific response of the learning network to task stages.

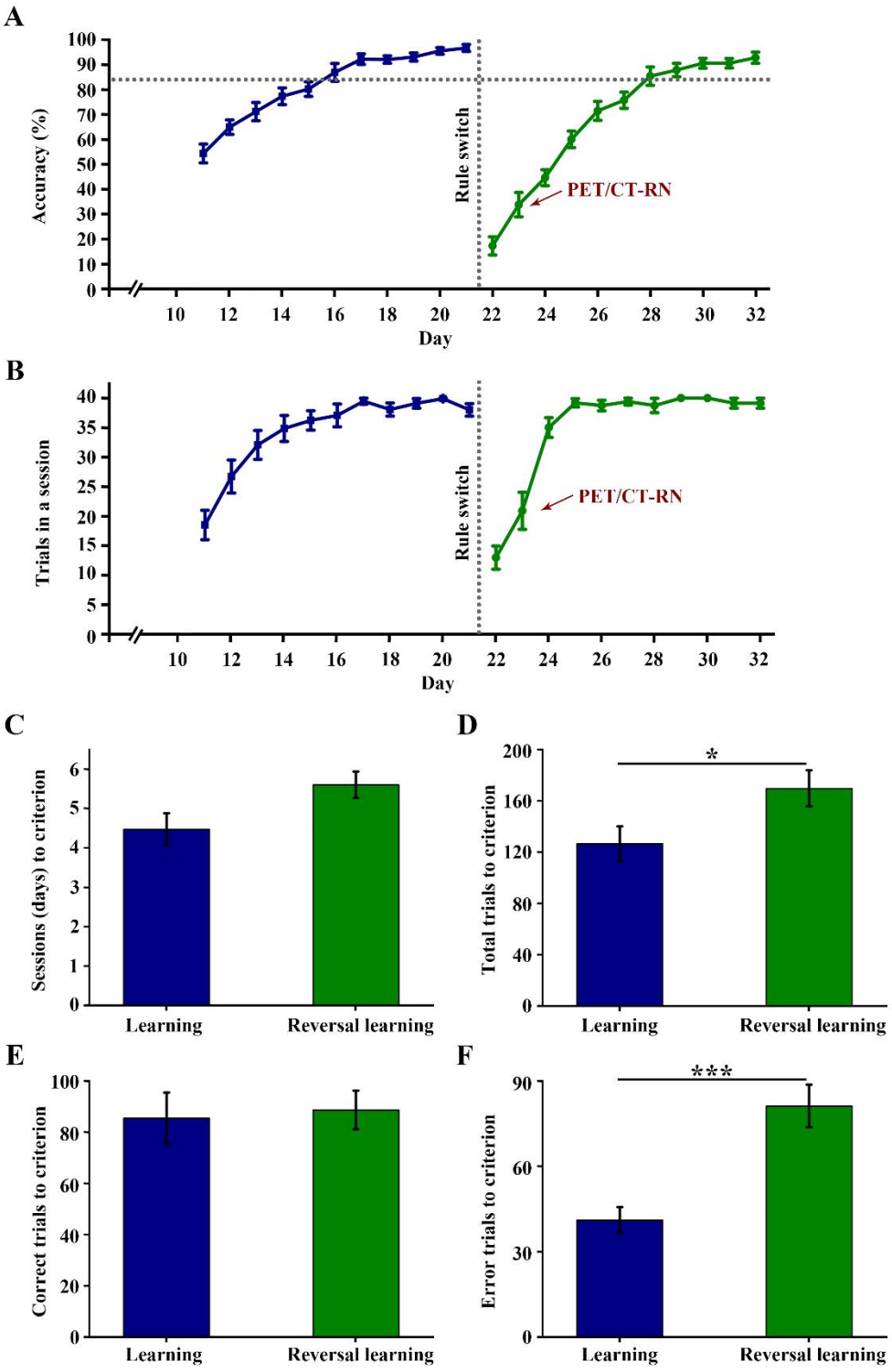

Supplementary Figure S1. Visual discrimination task behavioral performance in tree shrews. (A) Accuracy of each session. (B) Trial number in each session. (C) Number of training days, (D) total trials, (E) correct trials, and (F) error trials of tree shrews to reach task criteria. Error bars indicate standard errors. *P<0.05, ***P<0.001, Student's t-test.

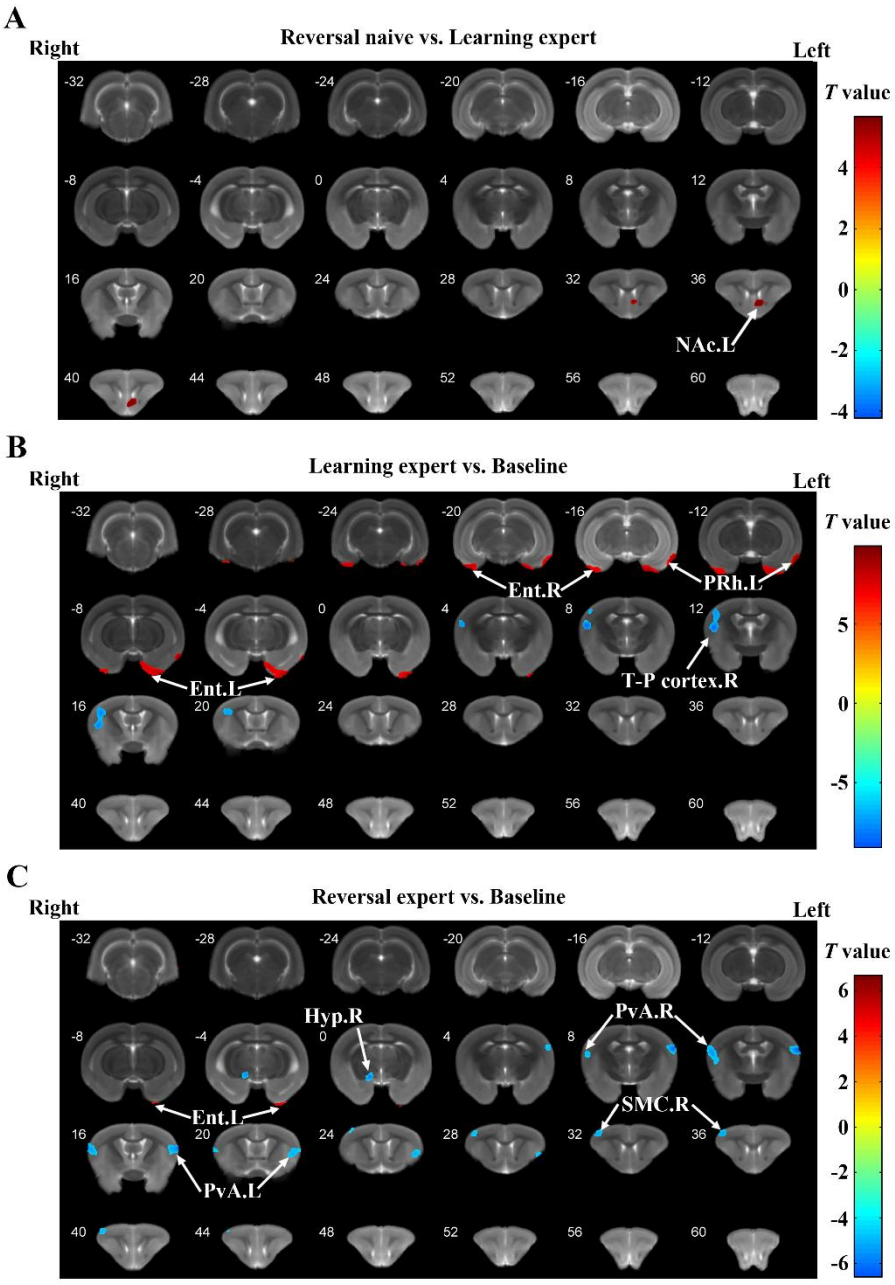

Supplementary Figure S2. Changes in glucose metabolism across different cognitive stages. (A) Voxel-wise comparison between RN and LE stage. Cluster with significant changes in glucose metabolism in RN state was located in left NAc (P<0.05, FWE-corrected, cluster size>50). (B) Voxel-wise comparison between LE and baseline stage. Clusters with significant changes in glucose metabolism in LE state were located in left Ent, left PRh, right Ent, and right temporal-parietal cortex (P<0.05, FWE, cluster size>50). (C) Voxel-wise comparison between RE and baseline stage. Clusters with significant changes in glucose metabolism in RE stage were located in left Ent, left PvA, right PvA, right Hyp, and right SMC (P<0.05, FWE-corrected, cluster size>50). Ent, entorhinal cortex; PRh, perirhinal cortex; T-P cortex, temporal-parietal cortex; NAc, accumbens nucleus; PvA, parietal ventral area; Hyp, hypothalamus; SMC, sensorimotor cortex. L, left hemisphere; R, right hemisphere.

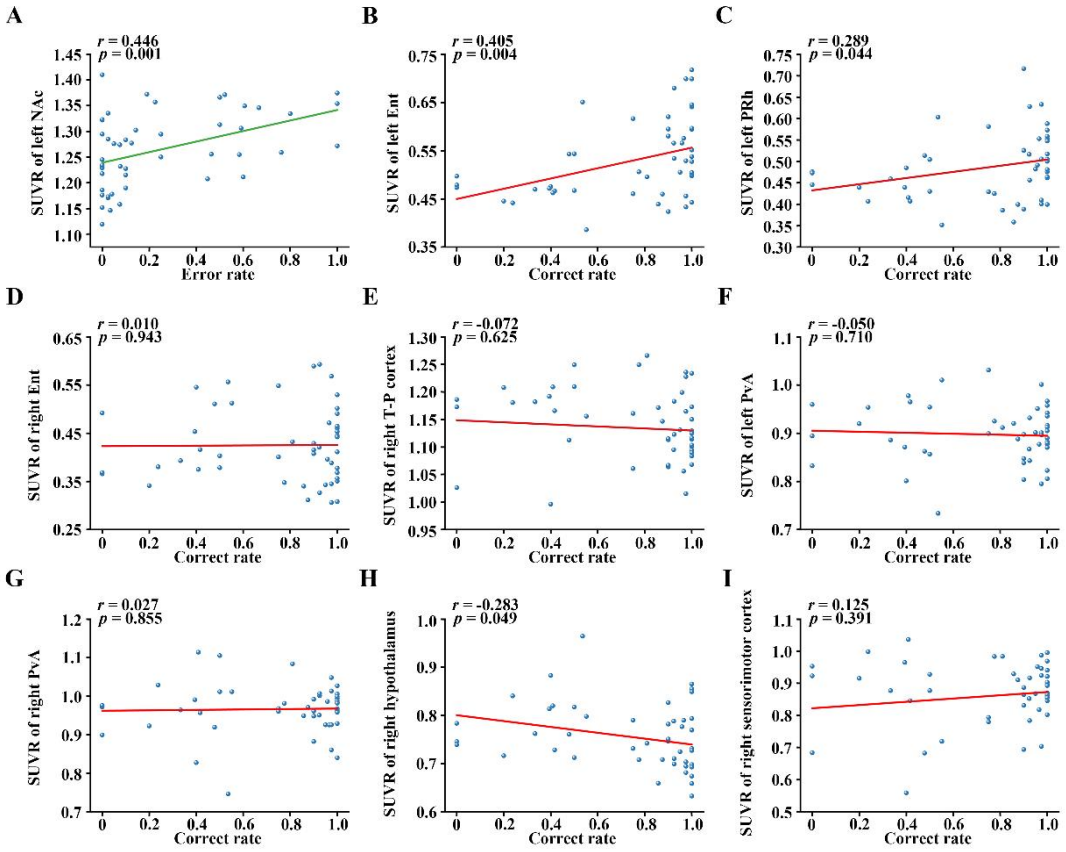

Supplementary Figure S3. Correlation between ^{18}F-FDG SUVR of brain clusters and measured behavior. SUVR, standard uptake value ratio, reference brain region was whole brain. Ent, entorhinal cortex; PRh, perirhinal cortex; T-P cortex, temporal-parietal cortex; NAc, accumbens nucleus; PvA, parietal ventral area; Hyp, hypothalamus; SMC, sensorimotor cortex. L, left hemisphere; R, right hemisphere. Pearson correlation analysis, significantly correlated parameters were set at $P<0.05$; r indicates Pearson correlation coefficient.

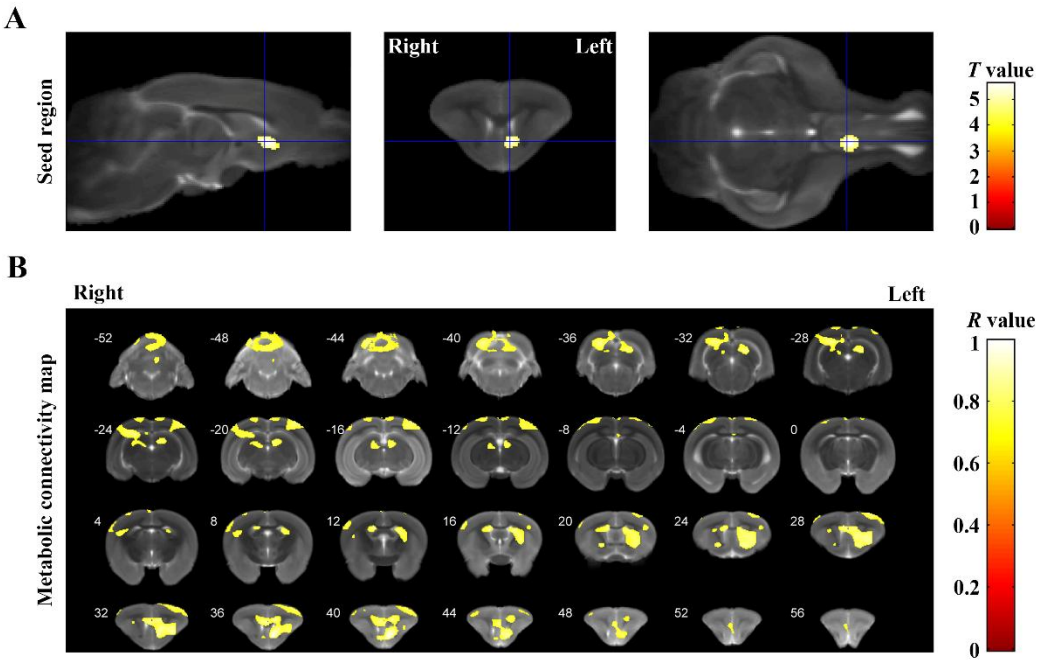

Supplementary Figure S4. Reversal learning metabolic network of tree shrew brain obtained in RN stage. (A) Left NAc was selected as a seed region. (B) Metabolic connectivity map of seed region in RN stage (P<0.05, FDR-corrected, cluster size>50). T value, value of two-sample t-test; R value, Pearson correlation coefficient.

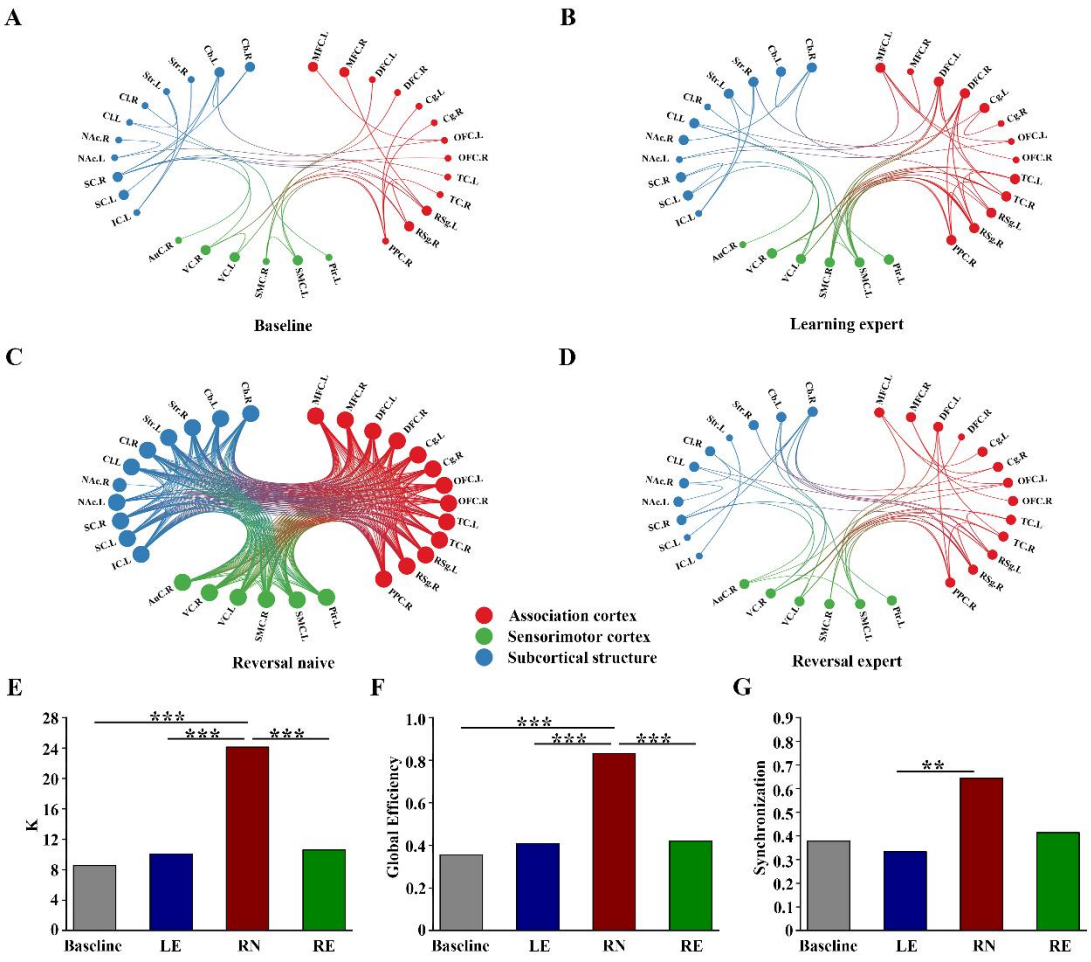

Supplementary Figure S5. Reversal learning (RL) network specifically responding to "rule-switch". Schematic of RL network metabolic connectivity in (A) baseline, (B) LE, (C) RN, and (D) RE stages. Size of ball indicates degree centrality of node. (E) Average network degree, (F) global efficiency, and (G) synchronization of RL network in four different cognitive stages. ***P*<0.01, ****P*<0.001, permutation test.

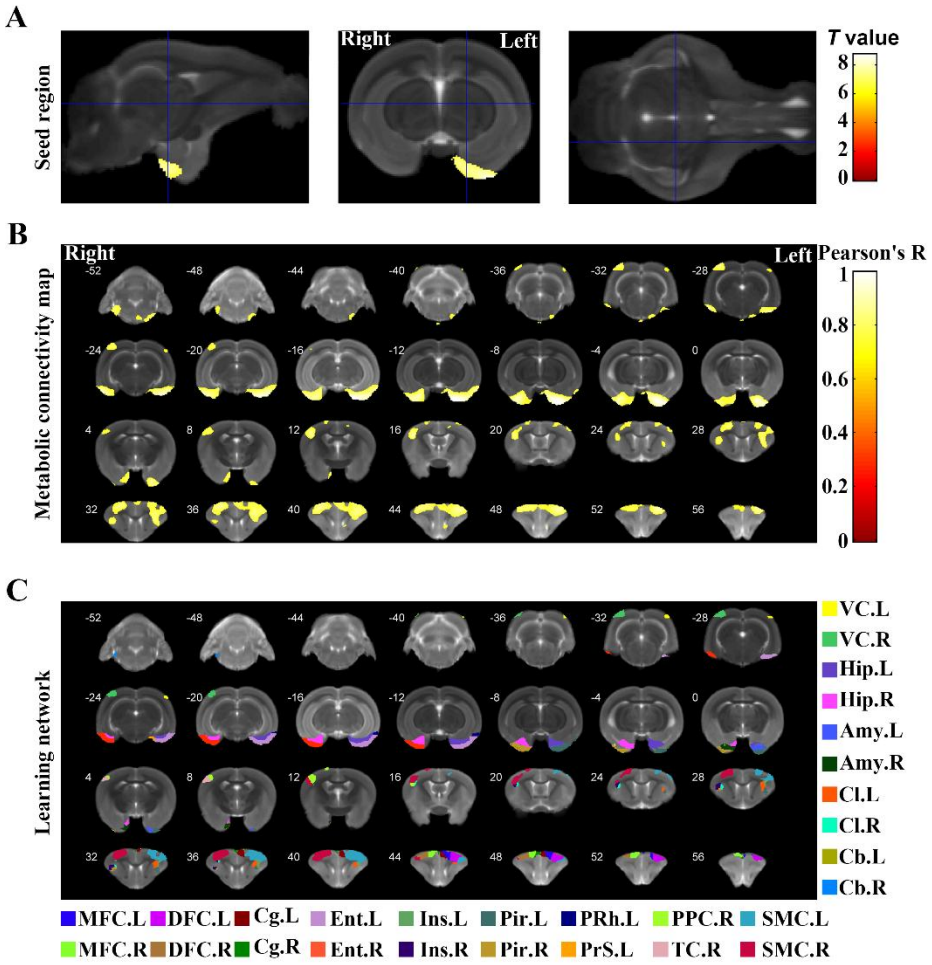

Supplementary Figure S6. Visual discrimination learning metabolic network of tree shrew brain obtained in LE stage. (A) Left entorhinal cortex was selected as a seed region. (B) Metabolic connectivity map of seed region in LE stage ($P<0.05$, FDR-corrected, cluster size>50). *T* value, value two-sample t-test; *R* value, Pearson correlation coefficient. (C) Sub-region location of visual discrimination learning network in tree shrew brain. Sub-functional region segmentation is presented in pseudocolor, whereas structural slices of tree shrew brains are presented in grayscale as background. Details on sub-functional regions are listed in bottom and right panels. MFC, medial frontal cortex; DFC, dorsal frontal cortex; Cg, cingulate cortex; Ent, entorhinal cortex; Ins, insular cortex; Pir, piriform cortex; PRh, perirhinal cortex; PrS, presubiculum; PPC, posterior parietal cortex; TC, temporal cortex; SMC, sensorimotor cortex; VC, visual cortex; Hip, hippocampus; Amy, amygdala; Cl, claustrum; Cb, cerebellum. L, left hemisphere; R, right hemisphere.

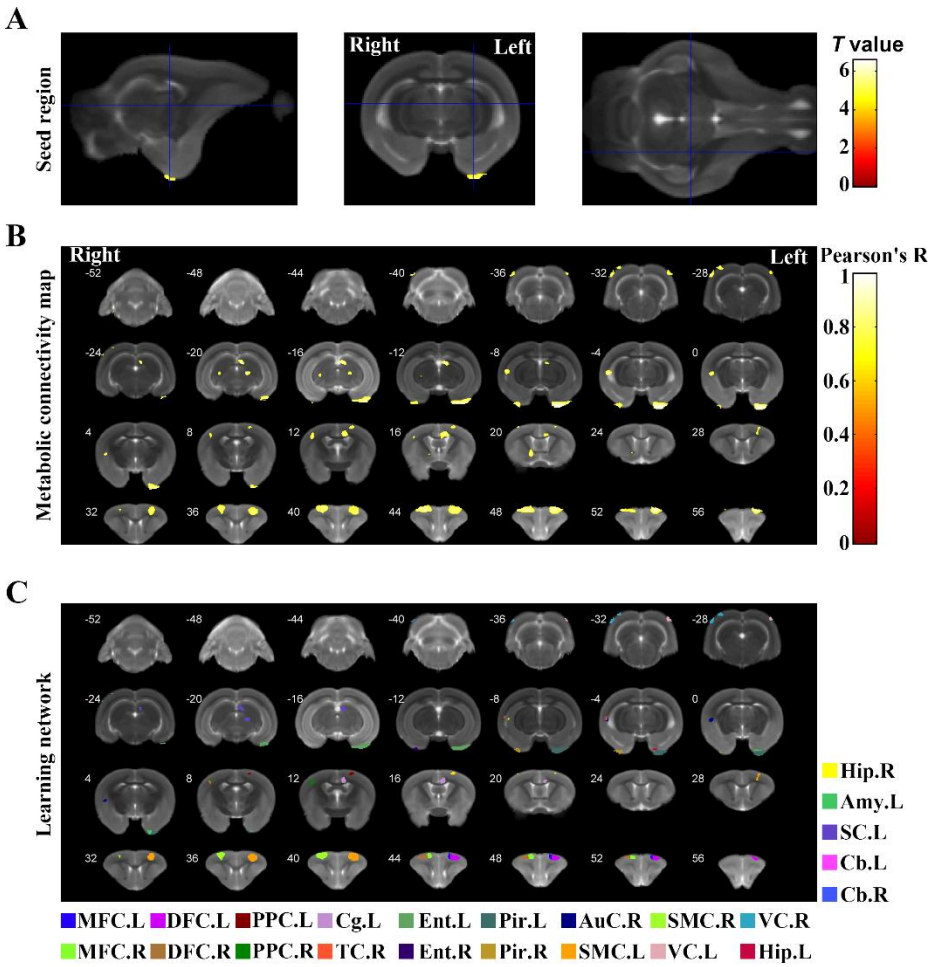

Supplementary Figure S7. Visual discrimination learning metabolic network of tree shrew brain obtained in RE stage. (A) Left entorhinal cortex was selected as a seed region. (B) Metabolic connectivity map of seed region in RE state (P<0.05, FDR-corrected, cluster size>50). T value, value of two-sample t-test; R value, Pearson correlation coefficient. (C) Sub-region location of visual discrimination learning network in tree shrew brain. Sub-functional region segmentation is presented in pseudocolor, whereas structural slices of tree shrew brains are presented in gray scale as background. Details on sub-functional regions are listed in bottom and right panels. MFC, medial frontal cortex; DFC, dorsal frontal cortex; Cg, cingulate cortex; Ent, entorhinal cortex; Pir, piriform cortex; AuC, auditory cortex; SC, superior colliculus; PPC, posterior parietal cortex; TC, temporal cortex; SMC, sensorimotor cortex; VC, visual cortex; Hip, hippocampus; Amy, amygdala; Cl, claustrum; Cb, cerebellum. L, left hemisphere; R, right hemisphere.

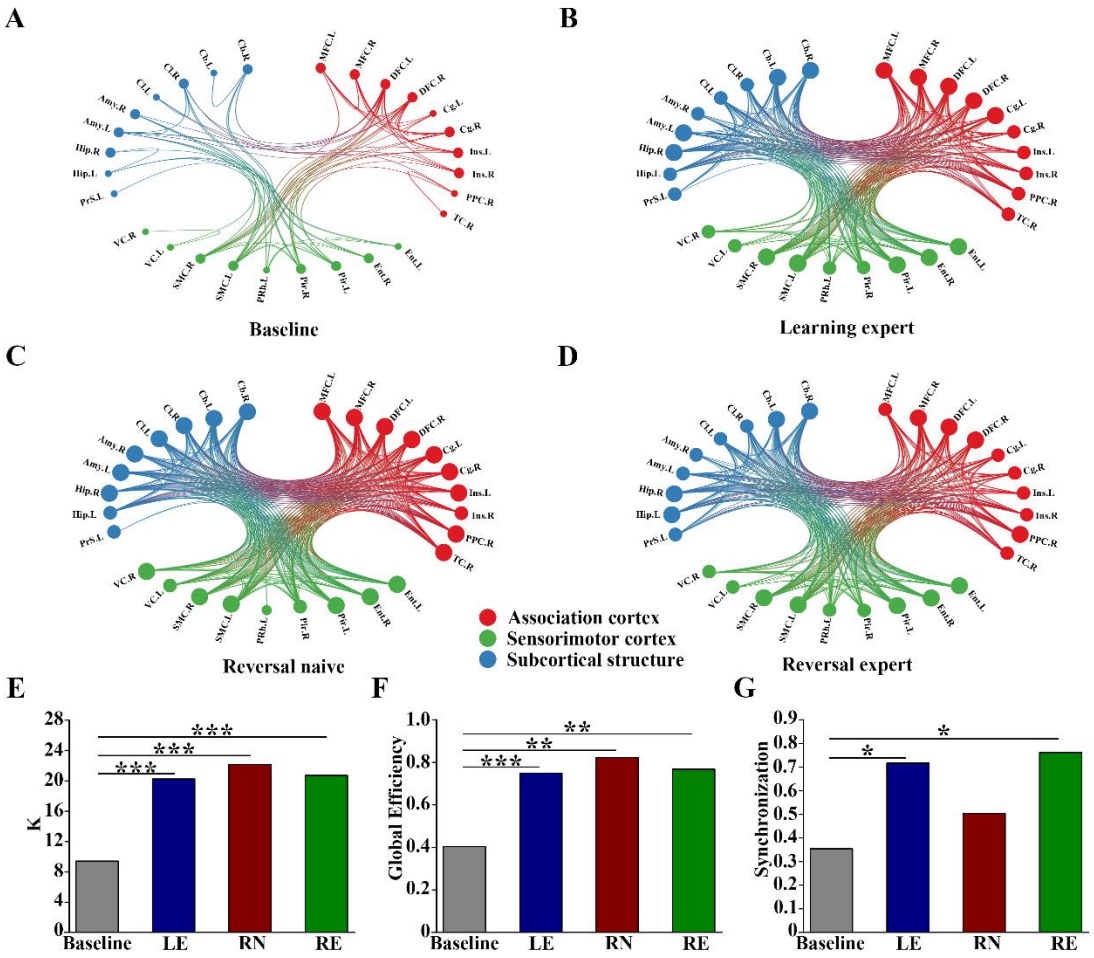

Supplementary Figure S8. Visual discrimination learning network specifically responding to task stages. Schematic of visual discrimination learning network metabolic connectivity in (A) baseline, (B) LE, (C) RN, and (D) RE stages. Size of ball indicates degree centrality of node. (E) Average network degree, (F) global efficiency, and (G) synchronization of visual discrimination learning network in four different cognitive stages. **P*<0.05, ***P*<0.01, ****P*<0.001, permutation test.

Supplementary Table S1. Significant changes in glucose metabolism in RN stage (RN vs. LE).

Region	Coordinate (mm)			Peak level		
	x	y	z	*T* value	*Z*-score	$P_{(FWE)}$
RN > LE						
Left accumbens nucleus	-1	7	4	5.62	4.80	0.006
RN < LE						
None						

Supplementary Table S2. Details on 30 brain structures in potential metabolic network associated with visual discrimination reversal learning. Nomenclature and abbreviations were adopted from histological atlas (L: left hemisphere, R: right hemisphere).

Brain regions	Abbreviations	Cluster size (mm^3)	Stereotaxic Coordinates (mm)		
			x	y	z
Medial frontal cortex	MFC.L	1320.86	-1	3	7
	MFC.R	1145.68	1	3	7
Dorsal frontal cortex	DFC.L	184.55	-4	4	7
	DFC.R	181.74	4	4	7
Cingulate cortex	Cg.L	373.78	-1	4	7
	Cg.R	441.22	1	4	7
Orbital frontal cortex	OFC	355.04	-1	6	7
	OFC	187.36	1	6	7
Temporal cortex	TC.L	511.48	-8	5	-4
	TC.R	1249.67	8	5	-4
Retrosplenial granular cortex	RSg.L	266.98	-1	3	-4
	RSg.R	1856.7	1	4	-4
Piriform cortex	Pir.L	799.08	-5	10	0
Posterior parietal cortex	PPC.R	414.99	6	2	-3
Sensorimotor cortex	SMC.L	3022.06	-4	2	1
	SMC.R	756.92	4	2	1
Visual cortex	VC.L	2956.48	-4	1	-6
	VC.R	3187.87	4	1	-6
Auditory cortex	AuC.R	148.95	8	8	-2
Inferior colliculus	IC.L	477.76	-2	7	-10
Superior colliculus	SC.L	2654.84	-3	5	-7
	SC.R	3053.91	3	5	-7
Accumbens nucleus	NAc.L	666.99	-1	7	4
	NAc.R	100.24	1	7	4
Claustrum	Cl.L	547.08	-3	5	4
	Cl.R	116.16	3	5	4

Striatum	Str.L	5802.43	-3	5	3
	Str.R	1200.95	3	5	3
Cerebellum	Cb.L	3728.39	-5	9	-11
	Cb.R	2238.91	5	9	-11

Supplementary Table S3. Significant changes in glucose metabolism LE stage (LE vs. baseline).

Region	Coordinate (mm)			Peak level		
	x	y	z	*T* value	*Z*-score	$P_{(FWE)}$
LE > Baseline						
Left entorhinal cortex	-5	14	-4	8.73	6.36	0.00
Left perirhinal cortex	-9	9	-6	8.51	6.26	0.00
Right entorhinal cortex	5	13	-5	7.87	5.96	0.00
LE < Baseline						
Right temporal-parietal cortex	7	5	-2	8.94	6.45	0.00

Supplementary Table S4. Details on 28 brain structures of potential metabolic network associated with visual discrimination learning obtained during LE stage. Nomenclature and abbreviations were adopted from histological atlas (L: left hemisphere, R: right hemisphere).

Brain regions	Abbreviations	Cluster size (mm^3)	Stereotaxic Coordinates (mm)		
			x	y	z
Medial frontal cortex	MFC.L	734.44	-1	3	7
	MFC.R	1099.78	1	3	7
Dorsal frontal cortex	DFC.L	1974.74	-4	4	7
	DFC.R	816.87	4	4	7
Cingulate cortex	Cg.L	1111.96	-1	4	7
	Cg.R	442.16	1	4	7
Entorhinal cortex	Ent.L	3726.52	-7	12	-6
	Ent.R	3077.33	7	12	-6
Insular cortex	Ins.L	310.07	-5	5	4
	Ins.R	559.26	5	5	4
Piriform cortex	Pir.L	2058.11	-5	10	0
	Pir.R	1551.31	5	10	0
Perirhinal cortex	PRh.L	492.75	-9	10	-5
Presubiculum	PrS.L	208.9	-5	10	-7
Posterior parietal cortex	PPC.R	974.25	6	2	-3
Temporal cortex	TC.R	368.16	8	5	-4
Sensorimotor cortex	SMC.L	5156.05	-4	2	1
	SMC.R	5183.21	4	2	1
Visual cortex	VC.L	354.1	-4	1	-6
	VC.R	1481.99	4	1	-6
Hippocampus	Hip.L	3905.44	-4	12	-5
	Hip.R	3241.27	4	12	-5
Amygdala	Amy.L	766.29	-4	12	-1
	Amy.R	1078.24	4	12	-1
Claustrum	Cl.L	989.24	-3	5	4

	Cl.R	298.83	3	5	4
Cerebellum	Cb.L	785.02	-5	9	-11
	Cb.R	1697.45	5	9	-11

Supplementary Table S5. Significant changes in glucose metabolism RE stage (RE vs. baseline).

Region	Coordinate (mm)			Peak level		
	x	y	z	*T* value	*Z*-score	$P_{(FWE)}$
RE > Baseline						
Left entorhinal cortex	-4	14	-4	5.19	4.39	0.05
RE < Baseline						
Left parietal ventral area	-8	5	0	6.50	5.15	0.002
Right hypothalamus	2	10	-3	6.32	5.06	0.004
Right parietal ventral area	8	5	-1	5.57	4.62	0.023
Right sensorimotor cortex	6	2	3	5.44	4.55	0.03

Supplementary Table S6. Details on 22 brain structures of potential metabolic network associated with visual discrimination learning obtained during RE stage. Nomenclature and abbreviations were adopted from histological atlas (L: left hemisphere, R: right hemisphere).

Brain regions	Abbreviations	Cluster size (mm^3)	Stereotaxic Coordinates (mm)		
			x	y	z
Medial frontal cortex	MFC.L	182.67	-1	3	7
	MFC.R	420.62	1	3	7
Dorsal frontal cortex	DFC.L	880.58	-4	4	7
	DFC.R	444.97	4	4	7
Cingulate cortex	Cg.L	461.83	-1	4	7
Entorhinal cortex	Ent.L	1378.00	-7	12	-6
	Ent.R	170.49	7	12	-6
Piriform cortex	Pir.L	1179.40	-5	10	0
	Pir.R	280.10	5	10	0
Auditory cortex	AuC.R	236.07	8	8	-3
Superior colliculus	SC.L	437.48	-3	5	-6
Posterior parietal cortex	PPC.R	171.43	6	2	-3
Temporal cortex	TC.R	100.24	8	5	-4
Sensorimotor cortex	SMC.L	1598.20	-4	2	1
	SMC.R	989.24	4	2	1
Visual cortex	VC.L	199.53	-4	1	-6
	VC.R	502.12	4	1	-6
Hippocampus	Hip.L	141.45	-4	12	-5
	Hip.R	100.32	4	12	-5
Amygdala	Amy.L	240.75	-4	12	-1
Cerebellum	Cb.L	108.99	-5	9	-11
	Cb.R	960.20	5	9	-11

REFERENCES

Barahona M, Pecora LM. 2002. Synchronization in small-world systems. *Physical Review Letters*, **89**(5): 054101.

Carbonell F, Charil A, Zijdenbos AP, Evans AC, Bedell BJ, Alzheimer's Dis Neuroimaging I. 2014. beta-Amyloid is associated with aberrant metabolic connectivity in subjects with mild cognitive impairment. *Journal of Cerebral Blood Flow and Metabolism*, **34**(7): 1169-1179.

Fan Y, Huang ZY, Cao CC, Chen CS, Chen YX, Fan DD, et al. 2013. Genome of the Chinese tree shrew. *Nature Communications*, **4**(1):1426.

Floresco SB. 2015. The nucleus accumbens: an interface between cognition, emotion, and action. *Annual Review of Psychology*, **66**, 25-52.

Güntürkün O, Ströckens F, Ocklenburg S. 2020. Brain lateralization: a comparative perspective. *Physiological Reviews*, **100**(3): 1019–1063.

Huang Q, Nie B, Ma C, Wang J, Zhang T, Duan S, et al. 2018. Stereotaxic F-18-FDG PET and MRI templates with three-dimensional digital atlas for statistical parametric mapping analysis of tree shrew brain. *Journal of Neuroscience Methods*, **293**: 105-116.

Huang Q, Zhang J, Zhang T, Wang H, Yan J. 2020. Age-associated reorganization of metabolic brain connectivity in Chinese children. *European Journal of Nuclear Medicine and Molecular Imaging*, **47**(2): 235-246.

Izquierdo A, Brigman JL, Radke AK, Rudebeck PH, Holmes A. 2017. The neural basis of reversal learning: an updated perspective. *Neuroscience*, **345**: 12-26.

Mar AC, Horner AE, Nilsson SRO, Alsioe J, Kent BA, Kim CH, et al. 2013. The touchscreen operant platform for assessing executive function in rats and mice. *Nature Protocols*, **8**(10): 1985-2005.

Motter AE, Zhou CS, Kurths J. 2005. Enhancing complex-network synchronization. *Europhysics Letters*, **69**(3): 334-340.

Mustafar F, Harvey MA, Khani A, Arató J, Rainer G. 2018. Divergent solutions to visual problem solving across mammalian species. *eNeuro*, **5**(4): ENEURO.0167-18.2018.

Rubinov M, Sporns O. 2010. Complex network measures of brain connectivity: uses and interpretations. *Neuroimage*, **52**(3): 1059-1069.

Schumacher JW, McCann M, Maximov KJ, Fitzpatrick D. 2021. Selective enhancement of neural coding in V1 underlies fine discrimination learning in tree shrew. *bioRxiv*, doi: 10.1101/2021.01.10.426145.

Tsai P-J, Keeley RJ, Carmack SA, Vendruscolo JCM, Lu H, Gu H, et al. 2020. Converging structural and functional evidence for a rat salience network. *Biological Psychiatry*, **88**(11): 867-878.

Uddin LQ. 2021. Cognitive and behavioural flexibility: neural mechanisms and clinical considerations. *Nature Reviews Neuroscience*, **22**(3): 167-179.

Wang JH, Zuo XN, Gohel S, Milham MP, Biswal BB, He Y. 2011. Graph theoretical analysis of functional brain networks: test-retest evaluation on short- and long-term resting-state functional MRI Data. *Plos One*, **6**(7): e21976.

Yakushev I, Drzezga A, Habeck C. 2017. Metabolic connectivity: methods and applications. *Current Opinion in Neurology*, **30**(6): 677-685.